

Noncolocated Adaptive Attitude Control of a Planar Two-Body Linkage with Nonminimum-Phase Dynamics

Gerardo Cruz¹ and Dennis S. Bernstein¹

Abstract—Adaptive control of a two-dimensional model of a flexible spacecraft with noncolocated sensors and actuators is achieved by output feedback using knowledge of only the system’s impulse response. The model is composed of two planar rigid bodies linked by a torsional spring that emulates a multibody spacecraft with base body actuation and appendage pointing. Retrospective cost adaptive control is applied to a command-following problem. The controller uses a finite impulse response filter built from the Markov parameters of the nonminimum-phase (NMP) linearized model. Accordingly, this filter is constructed to contain an estimate of the location of the NMP zero; the filter’s order is chosen to correspond to the number of time steps after which the plant’s step response becomes positive.

I. INTRODUCTION

Attitude control of multibody systems is a long-studied problem that remains challenging due to uncertainty, non-linearity, and dimensionality. Uncertainty may arise due to imprecisely modeled mass and modal properties [1, 2]; non-linearity arises due to large-angle and high-rate kinematics; and high dimensionality is due to the continuum mechanics of flexible appendages [3] or propellant slosh [4].

To address this problem, we examine the performance of an adaptive attitude control law for a planar model of a multibody spacecraft. A related study [5] examined a rigid spacecraft with a single discrete flexible degree of freedom. The spacecraft considered in [5] consists of a rigid base body connected by a compliance to a proof mass that can move along a single direction relative to the base body. The motion of the proof mass is assumed to be unmodeled and unknown, thereby providing a spacecraft model with flexible-mode uncertainty. This model was used to evaluate the performance of an adaptive attitude control law based on retrospective cost adaptive control (RCAC) [6], [7], [8].

Simplified flexible models such as the two body system in [5] provide exact nonlinear models of a flexible spacecraft under arbitrary motion. These models can remove the need for a continuum model of flexible dynamics and thus provide a setting for assessing the baseline performance of attitude control laws applied to flexible spacecraft.

This paper follows the philosophy of [5] by formulating an idealized flexible spacecraft model that is amenable to exact modeling. We consider a planar spacecraft model consisting of two rigid bodies, in this case a base body and an articulated appendage. These bodies are connected by a compliance that allows in-plane relative rotation but no translation. The performance objective is to achieve attitude

pointing of the appendage with actuation applied to the base body; this model may represent a telescope mounted on a spacecraft bus.

This model presents a challenging problem since the actuation and performance variable are noncolocated. The implications of this control-system architecture are evident due to the fact that control torques applied to the base body to induce rotation in a given direction result in initial rotation of the appendage in the opposite direction. This phenomenon indicates NMP behavior.

Adaptive control of NMP plants remains a challenging problem [9]. As shown in [8], RCAC is applicable to NMP systems as long as the plant is either open-loop asymptotically stable or the NMP zeros are known. In [10], RCAC is applied to a linearized planar linkage with actuator/performance-variable noncolocation. However, unlike the linkage in [10], in this paper the base body’s translation is unconstrained. Since the system has a rigid body mode it is both unstable and NMP.

II. PLANAR TWO-BODY LINKAGE

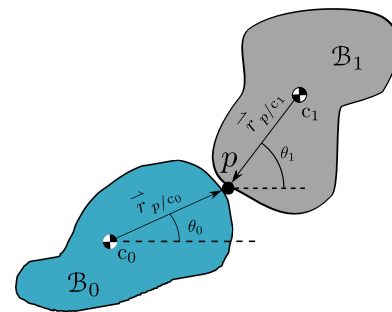


Fig. 1. Planar two-body linkage with base body \mathcal{B}_0 and appendage \mathcal{B}_1 . The angles θ_0 and θ_1 represent the attitude of \mathcal{B}_0 and \mathcal{B}_1 relative to a vector fixed in an inertial frame.

For example, the mechanism in Figure 1 is controlled by a torque actuator on the base body \mathcal{B}_0 attached by a torsional spring to the appendage \mathcal{B}_1 . Assume that the center of mass c of the linkage is unforced. Additionally, define three reference points: the center of mass c_0 of \mathcal{B}_0 , the center of mass c_1 of \mathcal{B}_1 , and the location p of the flexible joint connecting \mathcal{B}_0 and \mathcal{B}_1 .

Define an inertial frame F_1 . Furthermore, for $i = 0, 1$, define a frame F_i fixed to \mathcal{B}_i ; the physical rotation matrix that rotates F_1 to F_i is given by $\vec{R}_{i/1}$. Similarly, the angular velocity of F_i relative to F_1 is given by $\vec{\omega}_{i/1}$. The vector from c to c_i is given by $\vec{r}_{c_i/c}$, and the vector from c_i to

¹Department of Aerospace Engineering, University of Michigan, Ann Arbor, MI

p is given by \vec{r}_{p/c_i} . Finally, the mass of \mathcal{B}_i is m_i and its physical inertia matrix relative to its center of mass c_i is given by $\vec{J}_{i/c}$. Resolving the rotation matrices, inertias, angular velocities, and position vectors in F_i yields

$$R_i \triangleq \vec{R}_{i/1} \Big|_i = \begin{bmatrix} \cos \theta_i & -\sin \theta_i & 0 \\ \sin \theta_i & \cos \theta_i & 0 \\ 0 & 0 & 1 \end{bmatrix}, \quad (1)$$

$$\vec{\omega}_{i/1} \Big|_i = \omega_i e_3, \quad (2)$$

$$\vec{J}_{i/c_i} \Big|_i = \text{diag}(\alpha_i, \beta_i, J_i), \quad (3)$$

$$\vec{r}_{p/c_0} \Big|_0 = r_0 e_2, \quad \vec{r}_{p/c_1} \Big|_1 = -r_1 e_2, \quad (4)$$

where, for $i = 0, 1$, $\dot{\theta}_i = \omega_i$, $r_i > 0$ is the distance from c_i to p , and, for $j = 1, 2, 3$, e_j is the j th column of the 3×3 identity matrix.

The control objective is to use the actuator on \mathcal{B}_0 to align F_1 with a desired frame F_d . Given the planar nature of the problem, we can represent this using the angle θ_1 in Figure 1 and its desired value θ_d . Thus, the error angle is given by

$$y \triangleq \theta_1 - \theta_d, \quad (5)$$

where $-\pi < \theta_d \leq \pi$.

A. Lagrangian Dynamics

1) *Kinetic Energy*: The kinetic energy of \mathcal{B}_0 relative to c with respect to F_1 is given by

$$T_0 = \frac{1}{2} J_0 \omega_0^2 + \frac{m_0}{2} \left\| \overset{\bullet}{\vec{r}}_{c_0/c} \right\|^2. \quad (6)$$

Using the definition of the center of mass yields

$$\begin{aligned} \overset{\bullet}{\vec{r}}_{c_0/c} \Big|_c &\triangleq -\frac{1}{m_0 + m_1} \left(m_0 \overset{\bullet}{\vec{r}}_{c_1/C_0} + m_1 \overset{\bullet}{\vec{r}}_{c_0/c_0} \right) \\ &= -\frac{m_1}{m_0 + m_1} \left(\overset{\bullet}{\vec{r}}_{c_1/p} + \overset{\bullet}{\vec{r}}_{p/c_0} \right). \end{aligned} \quad (7)$$

Using the transport theorem to differentiate (7) with respect to F_1 and resolving in F_1 yields

$$\overset{\bullet}{\vec{r}}_{c_0/c} \Big|_1 = \frac{m_1}{m_0 + m_1} (r_1 \omega_1 R_1 + r_0 \omega_0 R_0) e_1. \quad (8)$$

Substituting (8) into (6) yields

$$\begin{aligned} T_0 &= \frac{1}{2} J_0 \omega_0^2 + \frac{m_0}{2} \left(\frac{m_1}{m_0 + m_1} \right)^2 \\ &\quad \cdot \left(r_0^2 \omega_0^2 + r_1^2 \omega_1^2 + 2r_0 r_1 \omega_0 \omega_1 \cos \tilde{\theta} \right), \end{aligned} \quad (9)$$

where $\tilde{\theta} \triangleq \theta_0 - \theta_1$. Similarly, the kinetic energy of \mathcal{B}_1 relative to c with respect to F_1 is given by

$$\begin{aligned} T_1 &= \frac{1}{2} J_1 \omega_1^2 + \frac{m_1}{2} \left(\frac{m_0}{m_0 + m_1} \right)^2 \\ &\quad \cdot \left(r_0^2 \omega_0^2 + r_1^2 \omega_1^2 + 2r_0 r_1 \omega_0 \omega_1 \cos \tilde{\theta} \right). \end{aligned} \quad (10)$$

Adding (6) to (10) yields the total kinetic energy

$$T = \frac{1}{2} J'_0 \omega_0^2 + \frac{1}{2} J'_1 \omega_1^2 + \gamma r_0 r_1 \omega_0 \omega_1 \cos \tilde{\theta}, \quad (11)$$

where

$$J'_0 \triangleq J_0 + \gamma r_0^2, \quad J'_1 \triangleq J_1 + \gamma r_1^2, \quad \gamma \triangleq \frac{m_0 m_1}{m_0 + m_1}. \quad (12)$$

2) *Potential Energy*: Assume that the torsional spring exerts zero torque when $\tilde{\theta} = 0$. Then the torsional spring potential is given by

$$U = \frac{k'}{2} \tilde{\theta}^2, \quad (13)$$

where $k' > 0$ is the spring stiffness.

3) *Lagrangian and Equations of Motion*: The Lagrangian for the linkage is given by

$$\begin{aligned} L &= T - U \\ &= \frac{1}{2} J'_0 \omega_0^2 + \frac{1}{2} J'_1 \omega_1^2 + \gamma r_0 r_1 \omega_0 \omega_1 \cos \tilde{\theta} - \frac{k'}{2} \tilde{\theta}^2. \end{aligned} \quad (14)$$

Since $\dot{\theta}_0 = \omega_0$ and $\dot{\theta}_1 = \omega_1$ the equations of motion are

$$\frac{d}{dt} \left(\frac{\partial L}{\partial \omega_0} \right) - \frac{\partial L}{\partial \theta_0} = u, \quad (15)$$

$$\frac{d}{dt} \left(\frac{\partial L}{\partial \omega_1} \right) - \frac{\partial L}{\partial \theta_1} = 0, \quad (16)$$

where $u \in \mathbb{R}$ is the control torque applied to \mathcal{B}_0 . Computing the partial derivatives (15) and (16) yields

$$J'_0 \dot{\omega}_0 + b_2 \dot{\omega}_1 + b_1 \omega_1^2 + k' \tilde{\theta} = u, \quad (17)$$

$$J'_1 \dot{\omega}_1 + b_2 \dot{\omega}_0 - b_1 \omega_0^2 - k' \tilde{\theta} = 0, \quad (18)$$

where

$$b_1 \triangleq \gamma r_0 r_1 \sin \tilde{\theta}, \quad b_2 \triangleq \gamma r_0 r_1 \cos \tilde{\theta}. \quad (19)$$

Combining (17) and (18) yields

$$M \begin{bmatrix} \dot{\omega}_0 \\ \dot{\omega}_1 \end{bmatrix} = \begin{bmatrix} k'E & 0_{2 \times 2} \end{bmatrix} x + b_1 \begin{bmatrix} -\omega_1^2 \\ \omega_0^2 \end{bmatrix} + \begin{bmatrix} 1 \\ 0 \end{bmatrix} u, \quad (20)$$

where $x = [\theta_0 \quad \theta_1 \quad \omega_0 \quad \omega_1]^T$,

$$M \triangleq \begin{bmatrix} J'_0 & b_2 \\ b_2 & J'_1 \end{bmatrix}, \quad E \triangleq \begin{bmatrix} -1 & 1 \\ 1 & -1 \end{bmatrix}. \quad (21)$$

Thus, the nonlinear equations of motion for the linkage are

$$\begin{aligned} \dot{x} &= \begin{bmatrix} 0_{2 \times 2} & I_2 \\ k'M^{-1}E & 0_{2 \times 2} \end{bmatrix} x \\ &+ \begin{bmatrix} 0_{2 \times 1} \\ M^{-1}b_1 \begin{bmatrix} -\omega_1^2 \\ \omega_0^2 \end{bmatrix} \end{bmatrix} + \begin{bmatrix} 0_{2 \times 1} \\ M^{-1} \begin{bmatrix} 1 \\ 0 \end{bmatrix} \end{bmatrix} u, \end{aligned} \quad (22)$$

where the inverse of the mass matrix is given by

$$M^{-1} = \frac{1}{J'_0 J'_1 - b_2^2} \begin{bmatrix} J'_1 & -b_2 \\ -b_2 & J'_0 \end{bmatrix}. \quad (23)$$

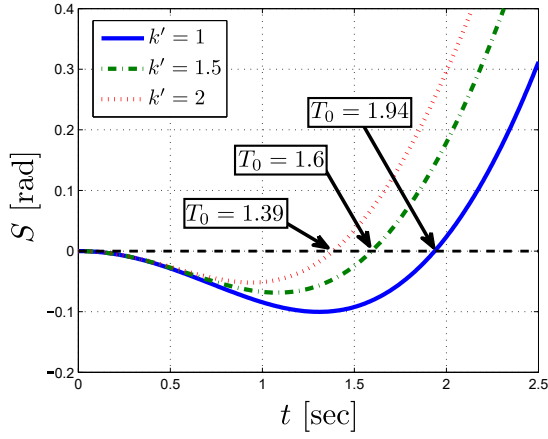


Fig. 2. Step response S for the nonlinear planar two-link mechanism for several values of the spring stiffness k' . For $i = 0, 1$, the model parameters are $r_i = 1$, $J_i = 1$, and $m_i = 1$; T_0 indicates each curve's zero-crossing time.

B. Dynamical Analysis

Subjecting the nonlinear system (22) to a unit step torque applied to \mathcal{B}_0 and measuring θ_1 yields the response in Figure 2. For all three stiffnesses, θ_1 begins negative, crosses zero, and then becomes and remains positive. This behavior indicates the presence of a NMP zero in the linearized dynamics as confirmed by linear analysis below.

1) *Linearization*: Computing the Jacobian of (22) at the equilibrium $\bar{x} = 0_{4 \times 1}$ yields

$$\delta \dot{x} = \begin{bmatrix} 0_{2 \times 2} & I_2 \\ k' \bar{M}^{-1} E & 0_{2 \times 2} \end{bmatrix} \delta x + \frac{1}{d} \begin{bmatrix} 0_{2 \times 1} \\ J'_1 \\ -\gamma r_0 r_1 \end{bmatrix} u, \quad (24)$$

$$y = [0 \quad 1 \quad 0 \quad 0] \delta x, \quad (25)$$

where $\delta x = x - \bar{x}$,

$$\bar{M}^{-1} \triangleq \frac{1}{d} \begin{bmatrix} J'_1 & -\gamma r_0 r_1 \\ -\gamma l_0 l_1 & J'_0 \end{bmatrix}, \quad d \triangleq J'_0 J'_1 - (\gamma r_0 r_1)^2. \quad (26)$$

Therefore, the transfer function for (24) and (25) is

$$G(s) = -\frac{\gamma r_0 r_1}{d} \frac{\left(s^2 - \frac{1}{\gamma r_0 r_1} k'\right)}{s^2 \left[s^2 + \frac{k'}{d} (J'_0 + J'_1 + 2\gamma r_0 r_1)\right]}. \quad (27)$$

Note that $G(s)$ contains the NMP zero

$$z_{\text{NMP}} = \frac{1}{\gamma r_0 r_1} \sqrt{k' \gamma r_0 r_1}. \quad (28)$$

C. Discretization

Discretizing the system matrix yields

$$A = e^{A_c h} \approx I_4 + h A_c = \begin{bmatrix} I_{2 \times 2} & h I_2 \\ h k' \bar{M}^{-1} E & I_2 \end{bmatrix}, \quad (29)$$

where h is the sample time and A_c is the system matrix (24). The input and output matrices are given by

$$B = \int_0^h e^{A_c \tau} d\tau \begin{bmatrix} 0_{2 \times 1} \\ B' \end{bmatrix} \approx \begin{bmatrix} \frac{h^2}{2} B' \\ h B' \end{bmatrix}, \quad (30)$$

$$C = [0 \quad 1 \quad 0 \quad 0], \quad (31)$$

respectively, where $B' = d^{-1} [J'_1 \quad -\gamma r_0 r_1]^T$.

We discretize (27) using the forward difference

$$G_{zu}(\mathbf{q}) = ch^2 \frac{\mathbf{q}^2 - 2\mathbf{q} + 1 - h^2 a}{(\mathbf{q} - 1)^2 [\mathbf{q}^2 - 2\mathbf{q} + 1 + bh^2]}, \quad (32)$$

where \mathbf{q} is the forward-shift operator and

$$a = \frac{1}{\gamma r_0 r_1} k', \quad b = \frac{k'}{d} (J'_0 + J'_1 + 2\gamma r_0 r_1), \quad c = -\frac{\gamma r_0 r_1}{d}. \quad (33)$$

Then taking the positive root of (32) yields the discrete-time NMP zero

$$z_{\text{NMP}} = 1 + h \sqrt{\frac{k'}{\gamma r_0 r_1}}. \quad (34)$$

III. RETROSPECTIVE COST ADAPTIVE CONTROL

RCAC is a discrete-time direct-adaptive controller; a detailed development is given in [7]. Define the performance variable

$$w(k) = y(k) - r(k), \quad (35)$$

where $r(k)$ is the reference. The n_c th order controller is given by

$$u(k) = \Phi(k) \Theta(k) \quad (36)$$

where

$$\Phi(k) \triangleq \begin{bmatrix} u(k-1) \\ \vdots \\ u(k-n_c) \\ w(k-1) \\ \vdots \\ w(k-n_c) \end{bmatrix}^T, \quad (37)$$

and the controller parameter $\Theta(k)$ is updated according to

$$\Theta(k) = \Theta(k-1) + L(k) [w'(k) - X(k) \Theta(k-1)], \quad (38)$$

$$\mathcal{P}(k) = [I - L(k) X(k)] \mathcal{P}(k-1), \quad (39)$$

where

$$L(k) = \mathcal{P}(k-1) X(k)^T \Gamma(k)^{-1}, \\ \Gamma(k) = R(k)^{-1} + X(k) \mathcal{P}(k-1) X(k)^T,$$

$$X(k) \triangleq \begin{bmatrix} \Phi_f(k) \\ \Phi(k) \end{bmatrix}, \quad w'(k) \triangleq \begin{bmatrix} u_f(k) - w(k) \\ 0 \end{bmatrix}.$$

and $R(k)$ regulates adaptation speed. The filtered regressor Φ_f is obtained by applying G_f to $\Phi(k)$ in (37). Constructing G_f is discussed in the following section.

IV. FILTER SELECTION

A. Laurent Expansion

The transfer function G_{zu} can be approximated using a truncated Laurent series outside a disk whose radius is the spectral radius of G_{zu} . The coefficients of this series are the Markov parameters [11]. We can use the Laurent series and the Markov parameters to estimate the location of the NMP zeros of G_{zu} ,

$$\begin{aligned} G_{zu}(\mathbf{q}) &\approx G_f(\mathbf{q}) \\ &= \frac{H_0 \mathbf{q}^{n_f} + H_1 \mathbf{q}^{n_f-1} + \dots + H_{n_f}}{\mathbf{q}^{n_f}} \\ &= \frac{(\mathbf{q} - \hat{z}_1) \dots (\mathbf{q} - \hat{z}_{n_{\text{NMP}}}) \dots (\mathbf{q} - \hat{z}_{n_f})}{\mathbf{q}^{n_f}}, \end{aligned} \quad (40)$$

where G_f is a filter built from the Laurent expansion of G_{zu} truncated after n_f terms, and for $i = 1, \dots, n_f$, \hat{z}_i is an approximate NMP zero, and n_{NMP} is the number of NMP zeros in G_{zu} .

The number of NMP zeros in G_f is a design parameter; Figure 3 shows that when the order of G_f is greater than n_{NMP} the additional zeros of G_f are distributed along the unit circle. If the plant is unstable, then G_f develops real and imaginary zeros as n_f increases. The triangular markers show that for $n_f = 9$ the zeros of G_f are all imaginary. As n_f increases, G_f develops a positive root as demonstrated when $n_f = 14$ and $n_f = 17$; for sufficiently large n_f , one of the real zeros of G_f approaches z_{NMP} (34).

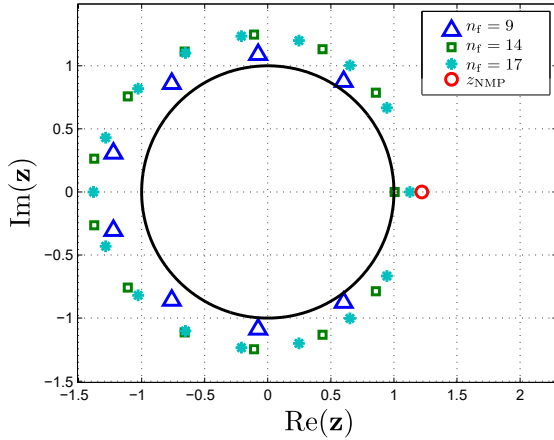


Fig. 3. Zeros of G_f (40) for several values of n_f and $k' = 2$. The location of G_{zu} 's NMP zero z_{NMP} (34) is represented by the small red circle to the right of the unit circle. As n_f increases, one of the zeros \hat{z}_i of (40) approaches the location of G_{zu} 's NMP zero z_{NMP} . For $i = 0, 1$, the model parameters are $r_i = 1$, $J_i = 1$, $m_i = 1$, and $h = 0.1$.

B. Step and Impulse response

The arrows in Figure 2 indicate the times where the step response changes sign for three different values of the spring stiffness k' . For the sampling time $h = 0.1$ sec, these times correspond to $k_0 = 14, 16, 19$ steps for $k' = 2, 1.5, 1$, respectively. Next, we examine whether the real zero in G_f is NMP given the filter order n_f .

Figure 4 shows that \hat{z} becomes NMP as n_f increases; specifically, \hat{z} becomes NMP after $k_0 = 14, 16, 19$. Thus, the minimum value of n_f needed to capture the NMP zero is related to the zero-crossings of the step response. For example, the solid line in Figure 2 indicates that the step response for $k' = 1$ is positive after $T_0 \approx 1.9$ sec which corresponds to

$$n_f \geq k_0 = hT_0 = 19. \quad (41)$$

We use (41) to construct G_f . In order to remove the need for the system's step response, we integrate the system's impulse response. The system's Markov parameters represent the impulse response; thus, summing the Markov parameters yields the step response of the system,

$$S(k) = \sum_{i=1}^k H_i. \quad (42)$$

Therefore, knowledge of the Markov parameters or experimentally obtaining the impulse response is sufficient to estimate capture the NMP properties of G_{zu} . By examining the behavior of the sum of the Markov parameters we can determine the minimum filter order needed to capture NMP zeros; specifically the filter order must satisfy

$$n_f \geq k_0. \quad (43)$$

The zero-crossing step k_0 is defined such that, for all $k \geq k_0$, the step response $|S(k)| > 0$. We use this empirical property to select G_f and apply it to the linkage problem using RCAC.

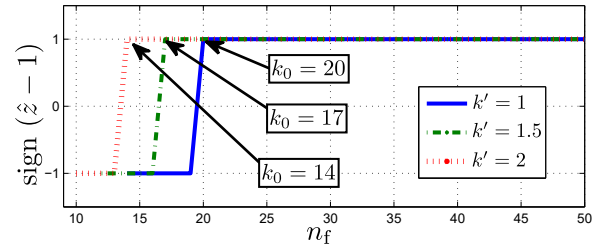


Fig. 4. Minimum-phase status of the estimated zero \hat{z} as a function of n_f for several stiffness values k' . The arrows with $k_0 > \frac{T_0}{h}$ indicate the first timestep at which the step response is positive. The plot shows that, if $n_f \geq k_0$, then \hat{z} is NMP. For $i = 0, 1$, the model parameters are $r_i = 1$, $J_i = 1$, $m_i = 1$, $c = 0$, and $h = 0.1$ sec.

V. NUMERICAL EXAMPLES

The following examples show a 180 degree step command where both rigid bodies start at rest and with zero angle error; this maneuver is intended to model a large-angle spacecraft slew. The model parameters are given by $r_0 = r_1 = 1$, $J_0 = 1$, $J_1 = 1$, $m_0 = m_1 = 1$, and $h = 0.1$.

A. Configuring RCAC

RCAC is configured using the Markov parameters to construct G_f . For the following examples we set $\Theta(0) = 0$, $R(k) = 0.1$, and $P(0) = 10^{10}$.

1) *Choosing n_f* : We examine the effect of increasing n_f so that the estimate of the NMP zero is closer to the true system value. We also compare the performance for various controller orders. Figure 5 shows that as n_f decreases the settling time increases. Additionally, if $n_f < k_0$, then $\theta(k)$ diverges. Thus, $G_f(q)$ must be NMP if the plant is NMP. Furthermore, increasing n_f reduces the settling time T_s and the steady-state error e_{ss} . Increasing n_c does not necessarily yield improved performance. However, close examination of the settling time and the steady-state error in Figure 5 suggests that performance improves in the case where the controller and filter orders match, that is, $n_f = n_c$. Given $n_c = n_f$, Figure 6 shows that the settling time and steady-state error decrease as n_f increases.

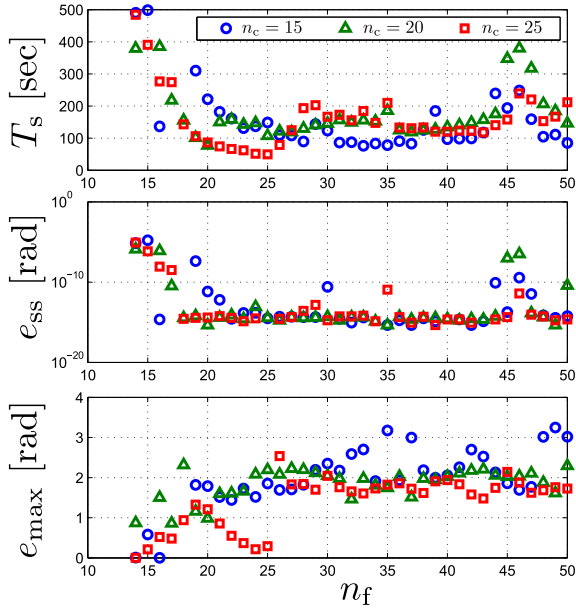


Fig. 5. Settling time T_s (top), steady-state error e_{ss} (middle), and overshoot e_{max} (bottom) as a function of the filter order n_f for a 180-deg step response; three different values for the controller order n_c are examined as shown by the differently shaped markers. Setting $n_c = n_f$ yields the best performance in each plot. The controller parameters are $R_u = 0.1$ and $R_\theta = 10^{-10}$. For $i = 0, 1$, the model parameters are $r_i = 1, J_i = 1, m_i = 1$, and $h = 0.1$.

B. Robustness Study

The examples in Figure 6 assume exact knowledge of the Markov parameters. Next we study the effect of uncertain parameters on performance.

1) *Parameter changes and the step response*: We examine how the system behavior changes as various parameters are scaled. For $i = 0, 1$, define a baseline two-body linkage whose parameters are given by $r_i = \bar{r}, J_i = \bar{J}, m_i = \bar{m}$, and $k' = \bar{k}'$; these parameters are then scaled one at a time. For example the stiffness is scaled as $k' = \alpha \bar{k}'$, where α is a positive constant; the mass, distance, and inertia are varied similarly. First, we examine the effect on the zero-crossing time T_0 in Figure 7. Note that the largest changes are due to variations in the spring stiffness k' and the distance r_i .

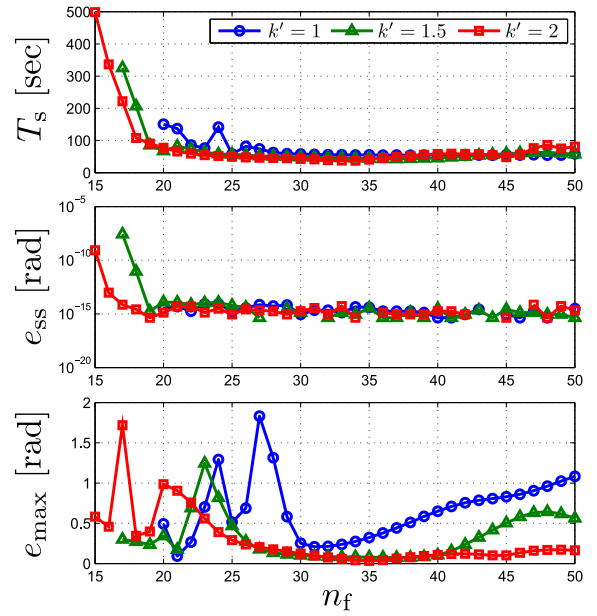


Fig. 6. Comparison of settling time T_s (top), steady-state error e_{ss} (middle), and overshoot e_{max} (bottom) as a function of the filter order n_f for the 180 degree R2R maneuver. The controller order $n_c = n_f$.

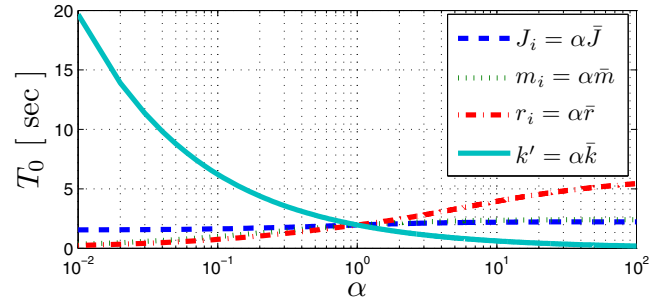


Fig. 7. Effect of parameter scaling on the step-response zero-crossing T_0 . The baseline parameters are $\bar{r} = 1, \bar{J} = 1, \bar{m} = 1, \bar{k}' = 1$.

The values of T_0 in Figure 7 can be used to select the minimum filter order for robustness to parameter scaling. For example, as k' increases, T_0 decreases. This suggests that a filter constructed for a smaller spring constant might provide sufficient information to account for the NMP behavior. Similar reasoning suggests that robustness to smaller than expected values of k' requires that n_f be large. The case of robustness to scaling of r_i is similar; as r_i decreases T_0 decreases, suggesting that performance of a filter chosen for larger r_i is acceptable.

2) *Response to scaled stiffness k' and distance r_i* : To test the robustness of the controller to uncertain plant information, we construct the filter G_f from the Markov parameters for the baseline system using $\bar{r}, \bar{J}, \bar{m}, \bar{k}'$. Independently scaling the stiffness or the center of mass location such that $k' = \alpha \bar{k}'$ or, for $i = 0$ or $i = 1$, $r_i = \alpha \bar{r}$ provides a method for testing robustness to modeling error. Figures 8 and 9 show the steady-state error e_{ss} and the maximum control input $\max|u|$ for the $\theta_d = 180$ deg R2R maneuver

in the case where either the stiffness k' or the center of mass locations r_0 or r_1 are uncertain.

In Figure 8, the stiffness is smaller than the nominal value and, since the step response crosses zero later than for $k' = 1$, the system is more difficult to control. In the case where the distance r_0 is less than the nominal distance RCAC can complete the maneuver; the step response crosses zero for values of r_0 less than $\bar{r} = 1$. In Figure 9, although the stiffness is larger than \bar{k} , the system is easier to control. Conversely, as the distance r_0 increases, RCAC is less able to stabilize the system.

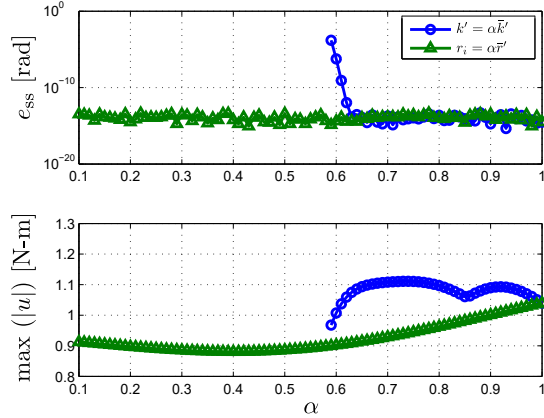


Fig. 8. Effect of parameter scaling on the R2R maneuver. The controller parameters are $n_f = n_c = 20$, $R(k) = 0.1$, $P(0) = 10^{10}$. The baseline parameters are $\bar{r} = 1$, $\bar{J} = 1$, $\bar{m} = 1$, $\bar{k}' = 1$.

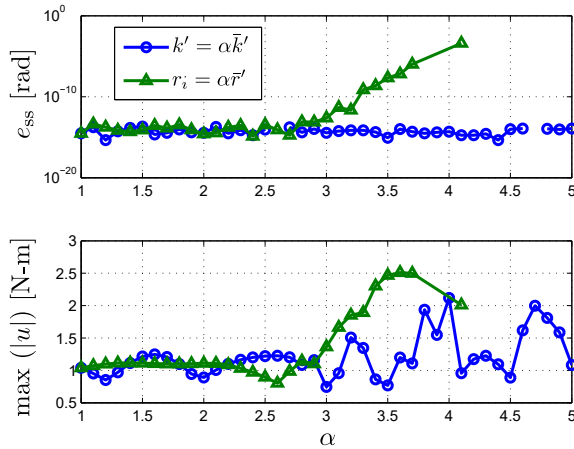


Fig. 9. Effect of parameter scaling on the R2R maneuver. The controller parameters are $n_f = n_c = 20$, $R(k) = 0.1$, $P(0) = 10^{10}$. The baseline parameters are $\bar{r} = 1$, $\bar{J} = 1$, $\bar{m} = 1$, $\bar{k}' = 1$.

VI. CONCLUSIONS

We considered command following for a two-body linkage with noncolocated sensors and actuators. Retrospective cost adaptive control enabled the application of a controller using minimal modeling information, namely the Markov parameters of the linearized system. Using the guidelines developed,

we constructed a controller that can robustly deal with the nonminimum-phase behavior and parameter uncertainty.

Although the Markov parameters can be obtained through linearization, they can also be estimated from the impulse response of the physical system, especially if a model is not readily available. The step response, which can be obtained by integrating the impulse response, provides the information needed to capture the NMP behavior of the system.

Numerical simulations show that using the zero crossing of the step response to determine the number of necessary Markov parameters results in an implementation of RCAC that is robust to scaling the spring stiffness and distance between the center of mass of either body to the flexible joint.

The techniques presented remain to be tested on the nonlinear model and a three-dimensional dual rigid body that models the dynamics of a multi-body spacecraft. Other practical considerations include saturation limits, which can be accommodated through a control penalty in the cost function, joint constraints that prevent the bodies from colliding with each other, and joint torsional damping which should make the system easier to control. A direct extension of this work would apply the guidelines in Section IV to other NMP systems.

REFERENCES

- [1] B. Xiao, Q. Hu, and Y. Zhang, "Fault-tolerant attitude control for flexible spacecraft without angular velocity magnitude measurement," *Journal of Guidance, Control, and Dynamics*, vol. 34, no. 5, pp. 1556–1561, 2011.
- [2] P. Gasbarri, "A two-dimensional approach to multibody free dynamics in space environment," *Acta Astronautica*, vol. 51, no. 12, pp. 831–842, 2002.
- [3] L. Vu-Quoc and J. C. Simo, "Dynamics of earth-orbiting flexible satellites with multibody components," *Journal of Guidance, Control, and Dynamics*, vol. 10, no. 6, pp. 549–558, 1987.
- [4] C. Nickkawde, P. Harish, and N. Ananthkrishnan, "Stability analysis of a multibody system model for coupled slosh-vehicle dynamics," *Journal of Sound and Vibration*, vol. 275, no. 3, pp. 1069–1083, 2004.
- [5] M. Cambor, A. Xie, G. Cruz, S. Esteban, T. Lee, and D. S. Bernstein, "A numerical comparison of inertia-free attitude control laws for a spacecraft with a discrete flexible mode," in *Proc. AIAA Guid. Nav. Contr. Conf.*, Boston, MA, August 2013, AIAA-2013-4562.
- [6] R. Venugopal and D. Bernstein, "Adaptive disturbance rejection using armarkov system representations," *IEEE Trans. Contr. Sys. Tech.*, vol. 8, pp. 257–269, 2000.
- [7] J. Hoagg, M. Santillo, and D. Bernstein, "Discrete-time adaptive command following and disturbance rejection with unknown exogenous dynamics," *Automatic Control, IEEE Transactions on*, vol. 53, no. 4, pp. 912–928, May 2008.
- [8] J. B. Hoagg and D. S. Bernstein, "Retrospective cost model reference adaptive control for nonminimum-phase systems," *AIAA J. Guid. Contr. Dyn.*, vol. 35, pp. 1767–1786, 2012.
- [9] D. Clarke, "Self-tuning control of nonminimum-phase systems," *Automatica*, vol. 20, no. 5, pp. 501–517, 1984.
- [10] A. Morozov, J. Hoagg, and D. Bernstein, "Retrospective cost adaptive control of a planar multilink arm with nonminimum-phase zeros," in *Decision and Control (CDC), 2010 49th IEEE Conference on*, Dec 2010, pp. 3706–3711.
- [11] M. A. Santillo and D. S. Bernstein, "Adaptive control based on retrospective cost optimization," *Journal of Guidance, Control, and Dynamics*, vol. 33, pp. 289–304, 2010.